Check for updates

Received: 23 March 2023 | Revised: 12 July 2023 | Accepted: 9 August 2023

DOI: 10.4218/etrij.2023-0112

SPECIAL ISSUE

ETRI Journal WILEY

Implementation of mmWave long-range backhaul for UAV-BS

Jangwon Moon[1] | **Junwoo Kim**[1] | **Hoon Lee**[1] | **Youngjin Moon**[1] | **Yongsu Lee**[1] | **Youngjo Bang**[1] | **Kyungyeol Sohn**[1] | **Jungsook Bae**[1] | **Kwangseon Kim**[2] | **Seungjae Bahng**[1] | **Heesoo Lee**[1]

[1]Mobile Communication Research Division, Electronics and Telecommunications Research Institute, Daejeon, Republic of Korea

[2]Radio Research Division, Electronics and Telecommunications Research Institute, Daejeon, Republic of Korea

Correspondence
Seungjae Bahng, Mobile Communication Research Division, Electronics and Telecommunications Research Institute, Daejeon, Republic of Korea.
Email: sjbahng@etri.re.kr

Funding information
Institute of Information & communications Technology Planning & Evaluation (IITP) grant funded by the Korea Government (MSIT) (2020-0-00045, Development of Movable High-Capacity Mobile Communication Infrastructure for Telecommunication Disaster and Rescue).

Abstract

Uncrewed aerial vehicles (UAVs) have become a vital element in nonterrestrial networks, especially with respect to 5G communication systems and beyond. The use of UAVs in support of 4G/5G base station (uncrewed aerial vehicle base station [UAV-BS]) has proven to be a practical solution for extending cellular network services to areas where conventional infrastructures are unavailable. In this study, we introduce a UAV-BS system that utilizes a high-capacity wireless backhaul operating in millimeter-wave frequency bands. This system can achieve a maximum throughput of 1.3 Gbps while delivering data at a rate of 300 Mbps, even at distances of 10 km. We also present the details of our testbed implementation alongside the performance results obtained from field tests.

KEYWORDS

flying base station, long-distance backhaul, millimeter wave, mobile backhaul, uncrewed aerial vehicle

1 | INTRODUCTION

Recently, many countries have announced the deployment of millimeter-wave (mmWave) 5G cellular systems. Although this frequency band is large, it suffers from high propagation loss, high directivity, and geographic constraints, leading to gaps in coverage. To overcome this, more 5G than 4G base stations (BSs) must be deployed close to users, resulting in increased capital and operating expenditures. To lessen this burden, the 3rd Generation Partnership Project (3GPP) is actively exploring the integration of nonterrestrial networks (NTNs) to extend the reach of networks from the ground to space, thereby enabling complete 5G service coverage for remote terrestrial areas. Moreover, owing to its geographically unconstrained nature, the NTN is well-suited for use in support of public safety, disaster relief, and emergency operations [1, 2].

NTN comprises three main components: satellites, high-altitude platform systems (HAPS), and uncrewed aerial vehicles (UAVs). Based on their operational altitudes, satellites are classified into geostationary, medium, and low-earth orbits (LEOs). HAPS are airborne platforms that operate in the stratosphere, and 3GPP is being used to explore their potential in providing mobile services using the same frequency bands as terrestrial

This is an Open Access article distributed under the term of Korea Open Government License (KOGL) Type 4: Source Indication + Commercial Use Prohibition + Change Prohibition (http://www.kogl.or.kr/info/licenseTypeEn.do).
1225-6463/$ © 2023 ETRI

networks. UAVs are essential components of NTNs and are versatile, rapidly deployed, and can hover for long periods in operational areas. UAVs provide low end-to-end latency compared with LEO satellites, which have around 100-ms latency (OneWeb.net), whereas the 3GPP (TS22.125) standard requires fewer than tens of milliseconds for most UAV applications [3]. Compared with satellites and HAPS, UAVs offer cost-effective solutions as they can be easily transported and deployed without extensive infrastructure investments. UAVs have already demonstrated their potential in various applications such as surveillance, construction inspection, package delivery, disaster monitoring, and search and rescue applications [4, 5].

Mounting a BS on a UAV, known as a UAV-BS, is being recognized as a practical solution for providing temporary cellular services in areas where traditional communication networks may be unavailable or disrupted, such as disaster relief operations [6, 7], temporary digital hotspots, and battlefield network coverage. To establish connectivity with core networks, the UAV-BS requires a wireless backhaul link, which can be established using technologies like long-term evolution (LTE), 5G-NR integrated access backhaul (IAB), or free space optics (FSO).

The feasibility of repurposing existing LTE BSs as backhaul connectivity for UAV-BS was demonstrated in Castellanos and others [8] for a real-world scenario, where the backhaul network, operating in the 3.5 GHz frequency band, and the access network, operating in the 2.5 GHz frequency band, were both implemented using LTE technology. Another study [9] used stochastic geometry to analyze LTE backhaul capabilities using UAV-BSs in urban environments, showing that a lower density of dedicated ground stations can yield satisfactory performance, whereas collocating these ground stations with existing BS networks provides additional LTE backhaul benefits.

The 5G-NR IAB [10] utilizes a portion of the radio spectrum for backhaul connections while reusing normal 5G-NR functions in support of flexible and widespread BS deployments without the need for substantial terrestrial infrastructures. In Fouda and others [11], the integration of UAV-BSs in a 5G-NR IAB scenario was investigated for its performance implications, resulting in a novel framework that optimizes network performance by minimizing congestion and maximizing user quality of service. The results demonstrated improvements in the average signal-to-interference-plus-noise ratio (SINR) per user and overall network throughput. In another study [12], the authors developed a deep reinforcement learning algorithm that optimizes the 3D placement of multiple UAV-BSs in a scenario where a macro BS is unavailable, and 5G-new radio (NR) IAB technologies were wielded to provide coverage in a disaster area. The new algorithm ensured that the service requirements of throughput and drop rate are successfully met.

In Ansari and others [13], FSO communications were employed to increase the capacity of the backhaul link between a UAV-BS and terrestrial BS. They proposed a novel UAV-BS placement method for hotspot and disaster zones to maximize the number of users served while maintaining a line of sight (LoS) backhaul link. Their approach also facilitated simultaneous charging and communication capabilities, resulting in significant improvements in both data rate and hovering time. In Nath and others [14], to address weather-related limitations of FSO communications, a cognitive hybrid FSO/radio frequency (RF) system was proposed to optimize 6G mobile system backhaul operations. The proposal integrates cognitive radio technology with FSOs, offering improved link availability while effectively utilizing RF resources.

As the requirements for UAV-BS backhaul continue to evolve, existing wireless technologies do not always offer sufficient link capacities or communication ranges in certain scenarios, particularly during emergencies. Consequently, researchers are exploring new approaches and technologies such as mmWave backhaul links. Hence, the wireless mmWave backhaul capability is our primary objective in this study. Specifically, we aim to achieve a maximum throughput of 1.3 Gbps over a 2.5-km distance while maintaining a 300-Mbps data rate within a 10-km range. To achieve this, narrow beams capable of efficiently delivering energy over long distances are utilized, emphasizing precise beam alignments due to UAV-BS aerial movements. A comprehensive description of our testbed setup is provided alongside field test results, which confirm the system's functionality and performance.

The remainder of this paper is organized as follows. Section 2 provides an overview of the objective UAV-BS system and presents a service case. Section 3 focuses on the backhaul system. The performance of our mmWave backhaul link is presented in Section 4, and Section 5 discusses the field tests and results. Finally, in Section 6, we conclude this paper.

2 | SYSTEM DESCRIPTION

In cases where fixed mobile communication networks fail to function properly owing to the collapse of terrestrial communication infrastructures or sudden surges in data traffic are expected during emergency rescue, security, and recovery operations, there is an urgent need to rapidly deploy high-capacity mobile communication

22337326, 2023, 5, Downloaded from https://onlinelibrary.wiley.com/doi/10.4218/etrij.2023-0112 by Elect & Telecom Research, Wiley Online Library on [01/11/2023]. See the Terms and Conditions (https://onlinelibrary.wiley.com/terms-and-conditions) on Wiley Online Library for rules of use; OA articles are governed by the applicable Creative Commons License

infrastructures whenever needed. Thus, integrating a mobile communication small-cell BS into a UAV enables the combined UAV-BS to establish an instant communication infrastructure by generating 4G/5G cell coverage from the air.

The unrestricted mobility of UAVs is advantageous for various applications in public services, logistics, smart cities, factories, ports, and airports, where high-speed ($\geq$100 Mbps) and low-latency ($\leq$100 ms) communication capabilities [15] are essential. UAV-BS is particularly well-suited for public disaster relief services that operate in regions with poor communication infrastructure, such as mountains, coasts, islands, and areas affected by the ground collapse. In the event of a communication infrastructure collapse or in cases in which an additional communication link is required to handle massive data traffic in certain areas, UAV-BSs can fly or hover over the service area and establish 4G/5G cells on the ground. This enables users within the cell coverage to connect immediately to the public network with unlimited 4G/5G communication quality via the UAV-BS. For example, as shown in Figure 1, if a wildfire occurs over a large area in the mountains, firefighters and civilians in the field can use their smartphones to capture real-time 4 K, ultra-high definition (UHD) videos of the wildfire and stream them simultaneously to the service platform located at the fire station via the UAV-BS. This is possible even in situations in which legacy 4G communications may not be capable of handling high-data rate video streams (in 2021, the LTE uplink (UL) throughput for users in mountainous areas in Korea was maintained at an average of 16 Mbps [16]).

Our proposed UAV-BS system consists of a flying BS (FBS) and mobile backhaul (MBH) system that enables fast and efficient 4G/5G cell services for ground users in disaster zones. The FBS establishes an airborne cell site, and the MBH provides a high-capacity link between the FBS and the core network. The MBH terminal on the UAV is responsible for establishing and maintaining a high-capacity link with the MBH hub on the ground when the UAV-BS moves or hovers. This study focuses on technologies pertaining to the UAV-BS, given that telecommunications companies efficiently manage mobile communication core networks on the ground. Moreover, the core technologies of the MBH hub, apart from beam management, can be explained by those of the MBH terminals.

2.1 | UAV

The UAV used in this study is a tethered type in which an external power generator on the ground supplies power to the UAV via a cable. This design offers significant advantages, including prolonged flight times and the ability to carry heavier payloads. As illustrated in Figure 2, the UAV has eight propellers and can accommodate a maximum take-off weight of 50 kg, which allows a maximum payload of 15 kg. Its power generator provides continuous power of up to 10 kW. Communication between the ground control station (GCS) and UAV for system management and control uses a conventional wireless modem. The MBH terminal antenna, which has a beam width of 10°, is mounted on the UAV's gimbal.

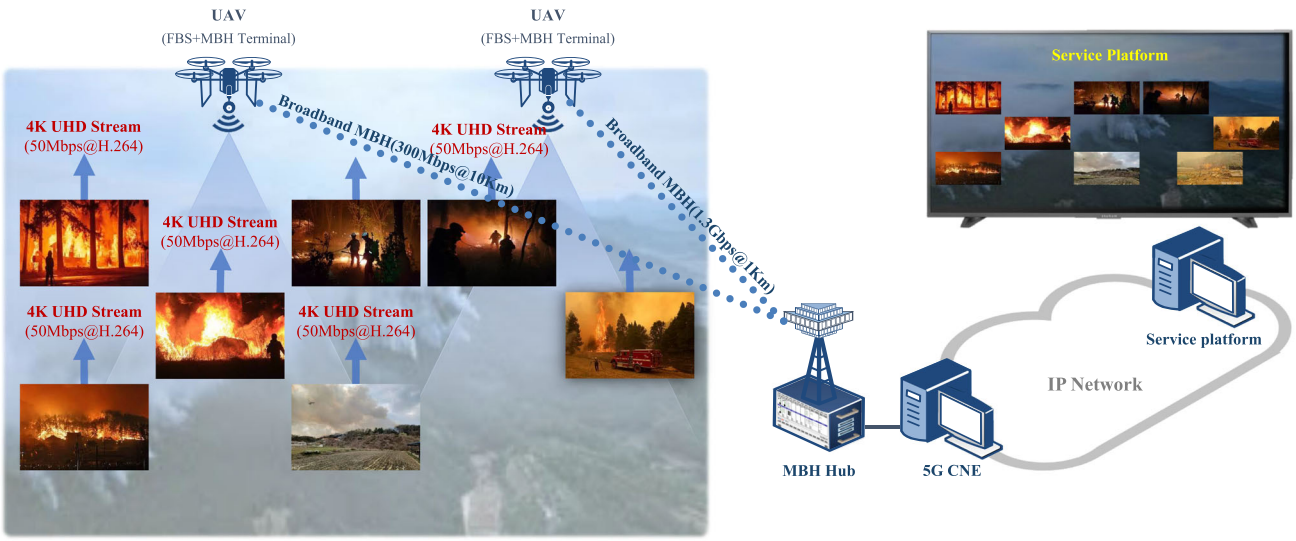

FIGURE 1 Example of an uncrewed aerial vehicle base station (UAV-BS) communication infrastructure for public disaster relief services.

22337326, 2023, 5, Downloaded from https://onlinelibrary.wiley.com/doi/10.4218/etrij.2023-0112 by Elect & Telecom Research, Wiley Online Library on [01/11/2023]. See the Terms and Conditions (https://onlinelibrary.wiley.com/terms-and-conditions) on Wiley Online Library for rules of use; OA articles are governed by the applicable Creative Commons License

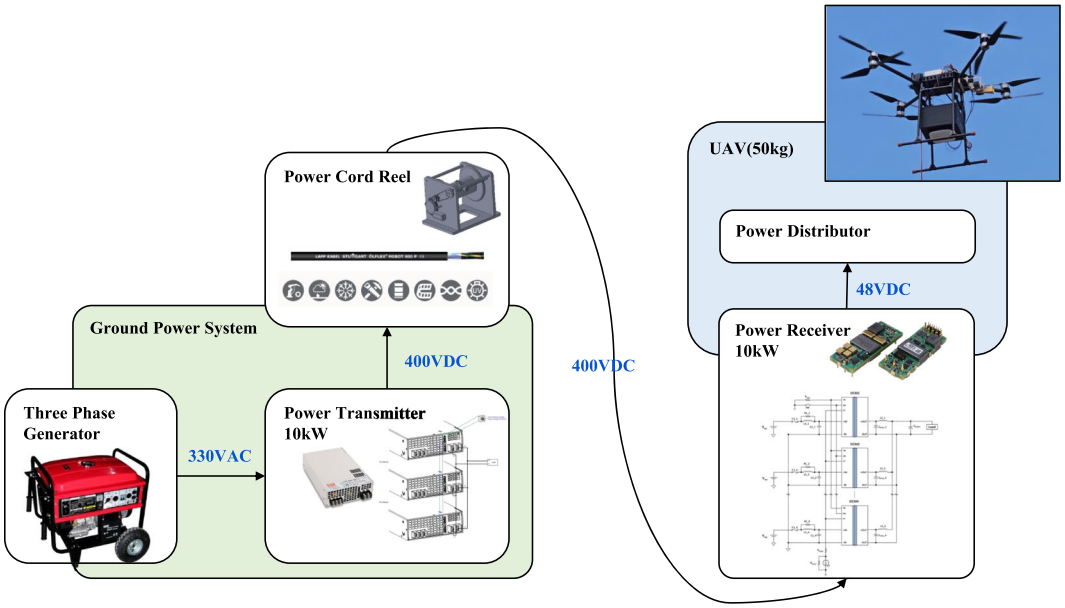

FIGURE 2 Architecture of the uncrewed aerial vehicle (UAV) for uncrewed aerial vehicle base station (UAV-BS) operations. A tethered UAV is used to supply consistent power from the ground.

Vertical antenna steering is accomplished by tilting the gimbal, whereas horizontal antenna steering is accomplished by rotating the UAV. This ensures that the antenna is optimally positioned to transmit and receive signals at all times.

2.2 | FBS

Our FBS is compliant with the 5G-NR FR1 stand-alone standard and utilizes polarized two-stream transmissions to achieve a data rate of 1 Gbps (256 QAM, code rate = 3/4, bandwidth (BW) = 100 MHz, and an n78 band). The FBS design minimizes size, weight, and power consumption to reduce the overall UAV load. We verified its performance against 3GPP TS 38.104 [17] using a 100-MHz BW in the 3550-MHz band, including power, frequency error, and ambient interference. Table 1 lists the hardware specifications of the FBS.

TABLE 1 Specifications of the flying base station (FBS).

Items	Values
Frequency range (GHz)	3.3–3.8 (5G-NR sub-6 n78)
Channel bandwidth (MHz)	100
Modulation order	256-QAM
Backhaul interface (Gbps)	10 (SFP+)
Volume (WDH cm^3)	3718 (= 26 × 26 × 5.5)
Net weight (kg)	2.2
Power consumption (W)	<68

2.3 | MBH

Our UAV integrates a high-speed MBH terminal to connect to the ground hub, thereby achieving a maximum 1.3-Gbps throughput using mmWave carriers. The MBH hub supports a standard 10-Gbps SFP+ interface to the network side to connect to the 4G/5G backbone.

The MBH system is operated in the 26.5 GHz–27.3 GHz mmWave band while utilizing a 400-MHz BW/link. Its carrier modulation employs 4096 orthogonal frequency division multiplexing (OFDM) with 120-kHz subcarrier spacing, and time division duplexing (TDD) is used to differentiate between UL and downlink (DL). Each MBH link supports a single stream data modulation of up to 64 QAM. Furthermore, it employs a low-density parity check (LDPC) error correction in data channels. Table 2 presents a comprehensive overview of the MBH system parameters.

The MBH frame structure is designed to effectively manage the available BW while maintaining a high-capacity backhaul link. The DL/UL switch occurs precisely once per midframe, which reflects the combination of the two subframes. Additionally, a full slot is designated null to support the establishment of backhaul links over distances of up to 10 km. Figure 3 shows the frame structure when the DL/UL ratio is set to 4:1. The MBH system is compatible with the 5G-NR system [18].

22337326, 2023, 5, Downloaded from https://onlinelibrary.wiley.com/doi/10.4218/etrij.2023-0112 by Elect & Telecom Research, Wiley Online Library on [01/11/2023]. See the Terms and Conditions (https://onlinelibrary.wiley.com/terms-and-conditions) on Wiley Online Library for rules of use; OA articles are governed by the applicable Creative Commons License

3 | MBH IMPLEMENTATION

The MBH hub and terminal are built on the same platform, which comprises a baseband modem, higher layers, and RF modules. However, the antennas and their associated components on the hub and terminal vary considerably as they are tailored to accommodate their respective radiation patterns and alignment mechanisms.

3.1 | Baseband modem

The baseband modem is implemented on the Xilinx Zynq UltraScale+ RF-SoC (XCZU48DR), which has several features, including eight 14-bit RF analog-to-digital conversion (ADC), digital-to-analog conversion (DAC), soft decision forward error correction (SD-FEC), multiple ARM core processing systems (PS), and FPGA programmable logic (PL) components. The PS is responsible for controlling the physical layer, setting the ADC/DAC, and interfacing with the higher layers. Most physical layer functions are implemented in the PL. To process a 400-MHz bandwidth, a 491.52-MHz system clock is required. However, standard FPGAs have difficulty accommodating these high clock frequencies. Consequently, our MBH modem operates at a lower clock frequency of 122.88 MHz, which is achieved by using four-path parallel processing in the modulator and demodulator.

To generate 14 OFDM symbols within the given slot duration using a coded transport block, a transmitter applies four parallel streams, each comprising a data mapper block that allocates data to physical channels and an inverse fast Fourier transform (IFFT) block that generates time-domain signals. At the receiver, the demodulator simultaneously processes four OFDM symbols, as does the transmitter. It uses a demodulation reference signal (DMRS) to estimate the wireless channel states and measures the phase noise using a phase-tracking reference signal to compensate for common phase errors. The demodulator generates log-likelihood ratio values that are serialized to satisfy the LDPC decoder interface. The relevant block diagram of baseband modem is shown in Figure 4.

The synchronization signal block (SSB) detection method is used for DL synchronization. This method consists of a matched filter for primary synchronization signal detection, a cell searcher for secondary synchronization signal detection, and a tracking unit [19]. The tracking unit uses DMRS. For UL synchronization in our MBH system, we use a physical random access

TABLE 2 Mobile backhaul (MBH) system parameters.

Items	Values
System bandwidth (MHz)	400
Occupied bandwidth (MHz)	368.64
Intermediate frequency (MHz)	3300
Radio frame duration (ms)	10
Midframe duration (ms)	2
Subframe duration (ms)	1
Slot duration (μs)	125
Number of orthogonal frequency division multiplexing (OFDM) symbols per slot	14
OFDM symbol duration (μs)	8.33
Number of subcarriers	3072
Subcarrier spacing (kHz)	120
Fast Fourier transform size	4096
Cyclic prefix (CP) length	288
CP duration (μs)	0.59
System clock (MHz)	122.88
ADC/DAC sampling frequency (MHz)	3932.16

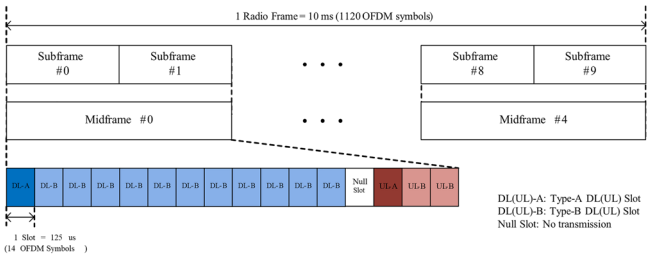

FIGURE 3 Frame structure and time-division duplex (TDD) configuration (DL:UL = 4:1).

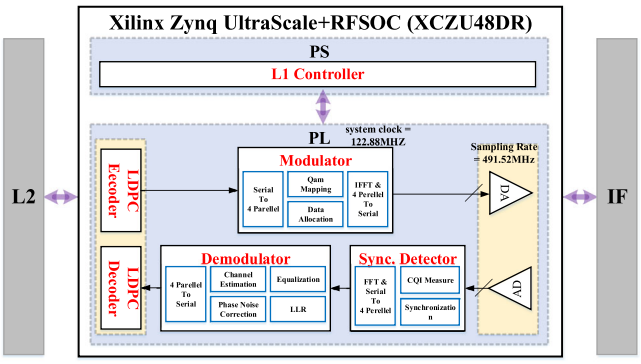

FIGURE 4 Block diagram of the mobile backhaul (MBH) baseband modem implemented on the Xilinx Zynq radio frequency (RF)-SoC (XCZU48DR).

22337326, 2023, 5, Downloaded from https://onlinelibrary.wiley.com/doi/10.4218/etrij.2023-0112 by Elect & Telecom Research, Wiley Online Library on [01/11/2023]. See the Terms and Conditions (https://onlinelibrary.wiley.com/terms-and-conditions) on Wiley Online Library for rules of use; OA articles are governed by the applicable Creative Commons License

channel (PRACH) [20] in the A3 format, which comprises a cyclic prefix and preamble sequence repeated six times. To use the PRACH for UL synchronization in a large cell radius of up to 10 km, its guard region is extended for 50 us. This corresponds to an approximate six symbol duration length, which is necessary to accommodate the maximum expected propagation delay for the distance, and it is approximately 34 μs. Figure 5 illustrates the A3 format of our PRACH, which includes an extended guard region. In Figure 5, C represents the cyclic prefix with a length of 1728 samples, S represents the time region of PRACH sequence, which consists of 4096 samples, and G represents the extended guard region composed of null samples. The PRACH sequence in the frequency domain is a short preamble with a length of 139. To detect the PRACH sequence at the MBH hub, we utilize time-domain peak detection followed by appropriate filtering and frequency domain correlations.

Both the DL and UL synchronizers in our system measure the signal-to-noise ratio (SNR) for adaptive modulation and coding (AMC). Noise power is measured using the null subcarriers of the SSB for the DL and the sounding reference signal (SRS) for the UL. Signal power is measured by correlating the DL DMRS or UL SRS with predetermined values. Additionally, the measured SNR is used to verify time synchronization accuracy. Alongside SNR measurements, the synchronizers measure the received signal strength indicator (RSSI) to aid in initial antenna alignment and automatic gain control (AGC) functions. The DL synchronizer calculates the received DMRS power for AGC and ensures that the full-frame power is within a certain range to prevent failures that may arise due to synchronization errors. The DL synchronizer also confirms that the antenna alignment is accurate. Similarly, the UL synchronizer employs SRS power to verify antenna alignment.

The LDPC encoder and decoder are implemented using the SD-FEC cores present in the RF-SOC. As each SD-FEC core is capable of supporting an LDPC encoder or decoder for the LTE and 5G standards [21], we utilize seven SD-FEC cores to implement all required channel codecs. To achieve a processing speed of 1 Gbps or greater, we use four SD-FEC cores for the channel decoders in the data channel.

FIGURE 5 Modified physical random access channel (PRACH) format where the A3 format is modified to accommodate distances of up to 10 km.

3.2 | RF and antennas

Figure 6 presents a detailed block diagram of the RF system, which is used in the same manner for both the MBH hub and the terminal to ensure consistent UL and DL backhaul performance.

The RF system is divided into an intermediate frequency module (IFM) and an RF module (RFM) to account for the mechanical interface and cable loss, because precise beam steering of a high-gain antenna for long-distance transmission is necessary, and the antenna must be mounted on an external moving structure. The IFM controls the gain for AGC and transmit power control (TPC), which must be interworked with the baseband model. By contrast, the RFM is responsible for converting signals to the RF band, amplifying them, and handling the transmission and reception switching functions. A single-pole double-throw switch is employed to ensure a fast time-division duplex (TDD) operation. Table 3 summarizes the RF system characteristics.

Figure 7 shows the fabricated IFM and RFM. The IFM was manufactured using an FR4 multilayer board connected to a baseband modem via a board-to-board connector. The IF signals are separated into receive and transmit paths. To simplify the RFM interface, the direct

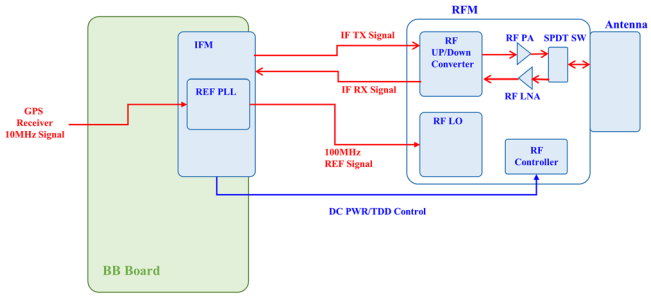

FIGURE 6 Block diagram of the proposed radio frequency (RF) system.

TABLE 3 Specifications of the proposed radiofrequency (RF) module.

Items	Values
Frequency (GHz)	26.5 to 27.3
IF (GHz)	3.3
Channel bandwidth (MHz)	400 × 2 FA
Output IP1dB (dBm)	27
Phase noise (dBc/Hz)	−89.2@10 kHz −96.7@100 kHz −107.7@1 MHz
TRx switching time (μs)	< 1

22337326, 2023, 5, Downloaded from https://onlinelibrary.wiley.com/doi/10.4218/etrij.2023-0112 by Elect & Telecom Research, Wiley Online Library on [01/11/2023]. See the Terms and Conditions (https://onlinelibrary.wiley.com/terms-and-conditions) on Wiley Online Library for rules of use; OA articles are governed by the applicable Creative Commons License

current power and TDD control signals are input to the IFM and connected through a single connector.

To improve the phase-noise characteristics of the RF, a 100-MHz reference signal for the RFM is provided using a phase-locked loop (PLL) circuit based on the reference signal, divided by the 10-MHz signal of the global positioning system (GPS) receiver. The control signal processing and RF signal parts of the RFM are spatially separated, and their sizes are optimized to reduce weight. The connection to the antenna uses a low-loss WR28 waveguide interface.

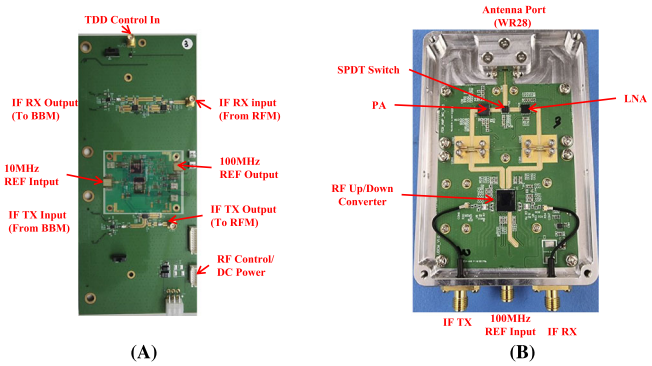

FIGURE 7 Radio frequency (RF) system implementation of (A) intermediate frequency module (IFM) and (B) RF module (RFM).

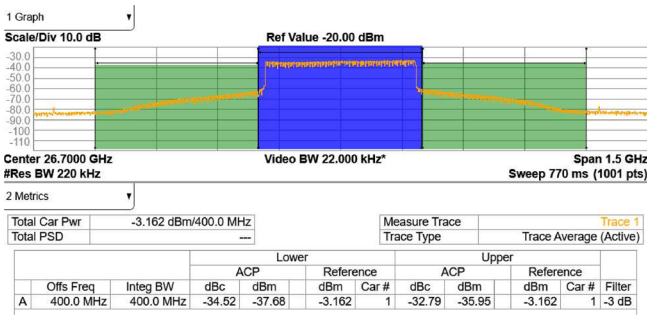

Measurement loss : 20dB Attenuator + 1m RF Cable(2.2dB Loss)

FIGURE 8 Output spectrum of radio frequency (RF) module at antenna port.

Figure 8 presents the RF output spectrum. The fabricated RFM has an adjacent channel power ratio (ACPR) greater than −32 dBc at a 19-dBm output with a 400-MHz 64-QAM OFDM signal. Figures 9 and 10 show illustrations and measurement results of the antennas. Because the MBH hub serves as a fixed station, it can operate stably; thus, a 35-dBi Cassegrain antenna with a 3-dB beamwidth of 2.2° is employed. To minimize the weight and overcome errors caused by vibrations, the MBH terminal antenna uses a 22.9-dBi horn antenna with a 3-dB beamwidth of 10.6°. The terminal antenna is vertically and linearly polarized, whereas the hub antenna is circularly polarized to maintain link quality, even when the terminal antenna tilts during movements or location controls.

3.3 | Beam alignment

To overcome the high propagation loss associated with the mmWave frequency band, it is necessary to transmit the signal with high power or use a narrow-beamwidth antenna to focus the limited transmission energy. Moreover, beam alignment techniques are needed to ensure backhaul service quality. The MBH hub continuously monitors the backhaul link state and adjusts the beam direction when it degrades.

Beam alignment is achieved via beam sweeps at the MBH hub. If the beam is misaligned, the modulation and coding scheme (MCS) of the backhaul is set to the lowest value (MCS0), and the MBH terminal send a calibration reference signal (Cal-RS) to measure the beam quality at

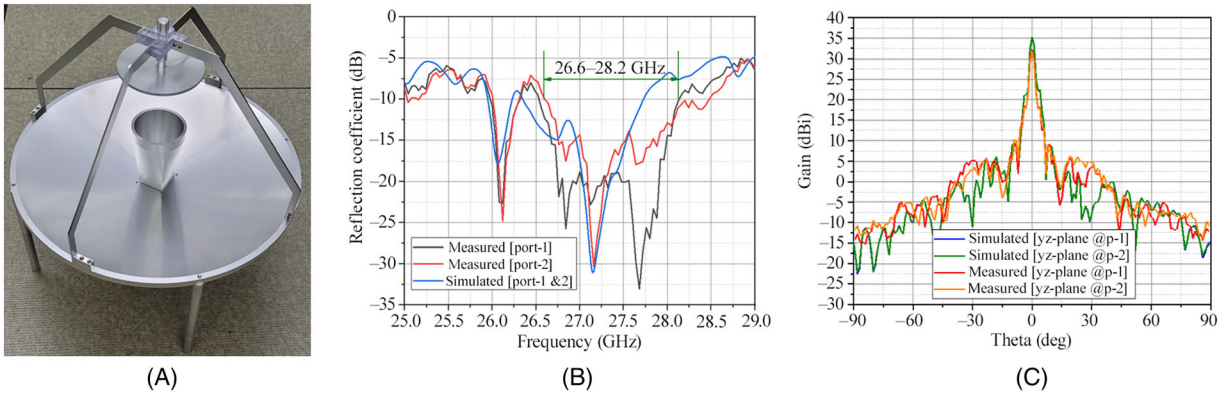

FIGURE 9 Mobile backhaul (MBH) hub antenna: (A) implementation, (B) return loss characteristic, and (C) radiation pattern.

22337326, 2023, 5, Downloaded from https://onlinelibrary.wiley.com/doi/10.4218/etrij.2023-0112 by Elect & Telecom Research, Wiley Online Library on [01/11/2023]. See the Terms and Conditions (https://onlinelibrary.wiley.com/terms-and-conditions) on Wiley Online Library for rules of use; OA articles are governed by the applicable Creative Commons License

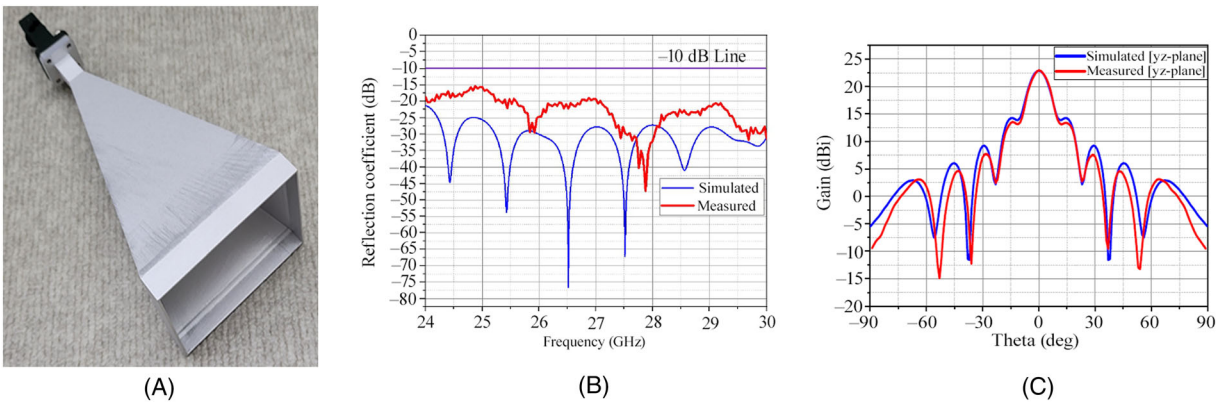

FIGURE 10 Mobile backhaul (MBH) terminal antenna: (A) implementation, (B) return loss characteristic, and (C) radiation pattern.

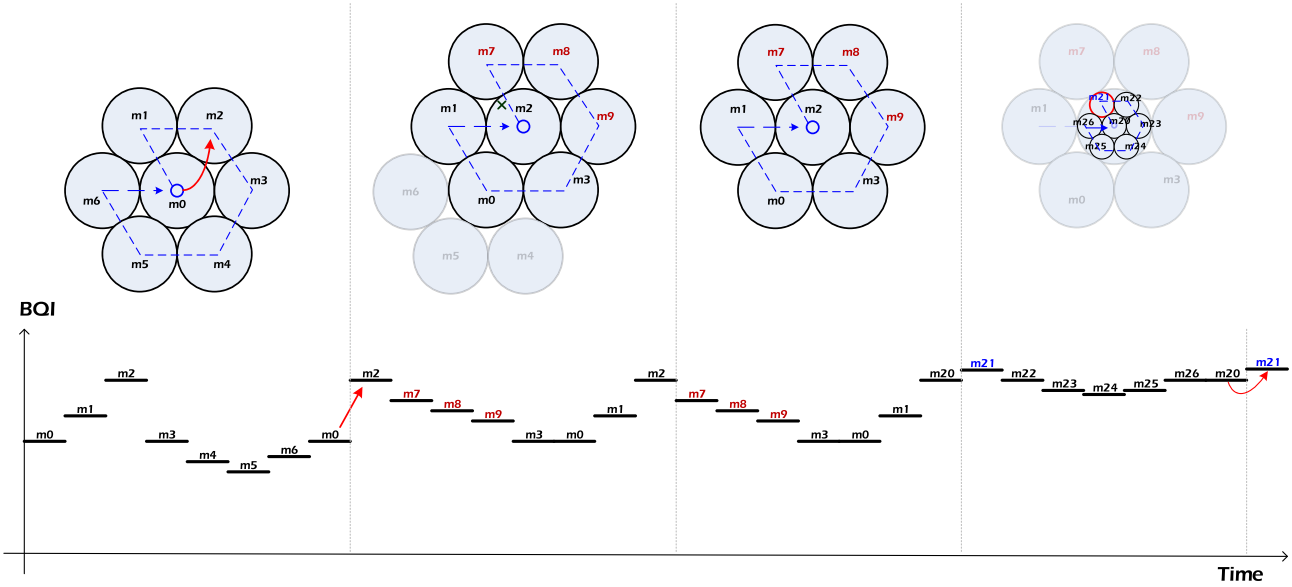

FIGURE 11 Example of beam alignment at the mobile backhaul (MBH) hub, where beam sweeping is achieved by scanning six points in the vicinity of the current position.

the MBH hub. Our implementation uses the UL SRS for Cal-RS. Figure 11 shows an example in which the beam quality is measured at each point by setting the radius around the current beam and conducting a beam sweep. If the beams at the same location exhibit the best beam quality in sequence, the sweep process is repeated while decreasing the radius at that the maximized point. Figure 11 illustrates the beam quality indication (BQI) measured using the UL SRS.

4 | MBH LINK PERFORMANCE

To determine the required SNR for each MCS, a link-level simulation was conducted using the system parameters specified in Table 2 without any impairments or degradations. The primary objective was to evaluate the maximum achievable throughput at a distance of 2.5 km, which is validated in Section 5 based on field tests. This section describes the determination of an achievable data rate for a distance of 10 km.

Table 4 presents the six MCSs employed in the MBH link, along with the corresponding achievable transmission rates when the DL/UL ratio is set to 4:1. Our MBH system achieved a transmission rate of up to 1.3 Gbps with MCS5 (64 QAM, code rate:0.75) and approximately 300 Mbps with MCS1 (QPSK, code rate:0.51).

Figure 12 shows the packet error rate (PER) for each MCS over a range of SNR values, revealing that a minimum SNR of 21 dB is required to achieve a PER of 1% or less using MCS5, whereas an SNR of approximately 7 dB is required for MCS1. During the simulation, we also

22337326, 2023, 5, Downloaded from https://onlinelibrary.wiley.com/doi/10.4218/etrij.2023-0112 by Elect & Telecom Research, Wiley Online Library on [01/11/2023]. See the Terms and Conditions (https://onlinelibrary.wiley.com/terms-and-conditions) on Wiley Online Library for rules of use; OA articles are governed by the applicable Creative Commons License

TABLE 4 MCS and achievable transmission rate (DL:UL = 4:1).

MCS index	Modulation order	Code rate R × 1024	Achievable transmission rate		
			Downlink	Uplink	Total
0	QPSK	251	113.26	28.31	141.57
1	QPSK	526	238.34	59.30	297.84
2	16 QAM	434	391.41	97.75	489.16
3	16 QAM	616	562.42	140.34	702.76
4	64 QAM	466	635.97	158.83	794.80
5	64 QAM	772	1051.72	262.68	1314.40

Abbreviation: MCS, modulation and coding scheme.

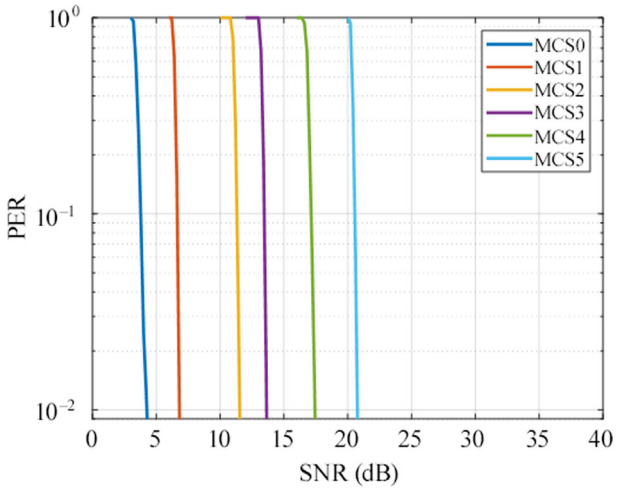

FIGURE 12 Plots of packet error rate as a function of the signal-to-noise ratio (SNR) for the mobile backhaul (MBH) link.

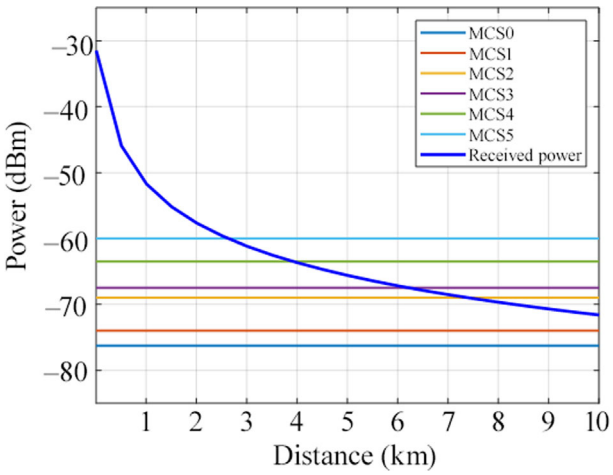

FIGURE 13 Plots of received power and sensitivity level at various modulation and coding scheme (MCS) values.

obtained the average error vector magnitude (EVM) at specific points of interest. This serves as a reference for indoor testing performance analysis when simulating long distances. Specifically, we obtained average EVMs of 19.7 dB and 20.5 dB for MCS5 at SNRs of 21 dB and 22 dB, respectively. The measured EVM should be within this range or higher to achieve a PER of less than 1%. For MCS1 with SNR values of 7 dB and 8 dB, the average EVM values were 3.8 dB and 5.2 dB, respectively.

In Section 3.2, we present the antenna gains of the MBH hub and terminal at 35 dBi and 22.9 dBi, respectively. For the link budget analysis, we utilized the free-space path loss (FSPL) model given in (1), where d denotes the distance between antennas, and f represents the frequency of the radio wave. Additionally, we considered a transmit power of 16.5 dBm to prevent clipping caused by the peak-to-average power ratio (PAPR), a 5-dB system margin, and a 7-dB noise figure. We conducted a comprehensive link budget evaluation using these parameters.

$$\mathrm{FSPL(dB)} = 20\log_{10}(d) + 20\log_{10}(f) - 147.55. \quad (1)$$

Figure 13 presents the received power and sensitivity levels of each MCS. We observed that MCS5 was supported within a distance of 2.5 km, and MCS1 was supported at a distance of 10 km.

We also conducted indoor tests to evaluate the performance of our MBH link by simulating distances of 10 km and 2.5 km. To simulate the path loss over a distance of 10 km, we connected the RF modules of the MBH hub and terminal using wires and inserted an 84-dB attenuator between them. We set the transmitter power to 16.5 dBm and measured the average EVM to be 12 dB, which was 6.8-dB higher than the required threshold of 5.2 dB. These results indicate that transmissions over a distance of 10 km are feasible with the proper alignment of the MBH hub and its terminal beams. For a distance of 2.5 km, where the path loss is 129 dB, we set the transmit power to 16.5 dBm and attenuation to 72 dB. The measured average EVM was 22.2 dB, indicating that data

22337326, 2023, 5, Downloaded from https://onlinelibrary.wiley.com/doi/10.4218/etrij.2023-0112 by Elect & Telecom Research, Wiley Online Library on [01/11/2023]. See the Terms and Conditions (https://onlinelibrary.wiley.com/terms-and-conditions) on Wiley Online Library for rules of use; OA articles are governed by the applicable Creative Commons License

transmissions at a rate of 1.3 Gbps are possible over a distance of 2.5 km. In Section 5, we demonstrate this using a field test. However, it is crucial to note that the optimal MBH performance depends on proper beam alignment. Misalignments can result in degraded signal quality, reduced data rates, or complete link failure.

5 | FIELD TESTS

To verify the functionality and performance of our UAV-BS system in diverse environments, we conducted field tests in the following order. 1. MBH link tests, where the MBH hub was installed on the ground, and the MBH terminal was mounted on an airborne UAV. 2. Communication link setup between the FBS mounted on the UAV and commercial user equipment (UE), specifically a Samsung Galaxy S20 located on the ground. 3. UAV-BS integration tests of mobile backhaul links to the core network. Detailed descriptions of the tests and their results are presented in the following sections.

5.1 | MBH link test

Precise beam alignment is crucial to optimizing MBH link performance. The process involves several key steps, including initial link establishment, beam alignment, and UAV tracking, in accordance with UAV movement. During the initial link setup, GPS data from the MBH hub are provided to the UAV. Subsequently, the MBH terminal antenna is attached to the UAV's gimbal, which points toward the MBH hub located on the ground. When the UAV reaches the target location, it searches for a synchronization signal sent by the MBH hub and executes the initial synchronization operation. The initial backhaul link setup is then finalized by transmitting the PRACH and configuring the timing advance value. Following the successful establishment of the backhaul link, the subsequent step involves beam alignment, as explained in Section 3.3. Subsequently, the MBH terminal periodically transmits its GPS information to the MBH hub and uses it to track UAV movements. The MBH hub continually monitors the backhaul link status and performs the beam alignment procedures as needed. All field tests were conducted in environments in which beam alignment was maintained.

We developed a modem control tool (MCT) and modem analysis tool (MAT) to remotely control the MBH modem and analyze the received baseband signal. MAT can be used to directly analyze the baseband signal at the MBH hub, producing various results. The MCT allows remote monitoring of the modem status and MBH terminal operations, taking advantage of an existing link through the GCS. Figure 14 illustrates the test environment, including the tools.

MBH link tests were performed at various distances and environments, as shown in Figure 15, to verify the effectiveness of beam alignment, impact of the surrounding environments on the backhaul link, and achievable data rate. The distances in Figure 15A–C correspond to 200 m, 400 m, and 2.5 km distances, respectively.

In the first test environment shown in Figure 15A, we successfully confirmed the efficacy of the initial beam alignment procedure, and the MBH hub antenna was able to track the UAV's movement in all directions. Despite a slight deterioration in the channel state caused by the scattering of surrounding bushes, we accurately obtained the predicted signal strength and achieved a peak data rate of 1.3 Gbps for MCS5 without errors, with an EVM of approximately 25 dB.

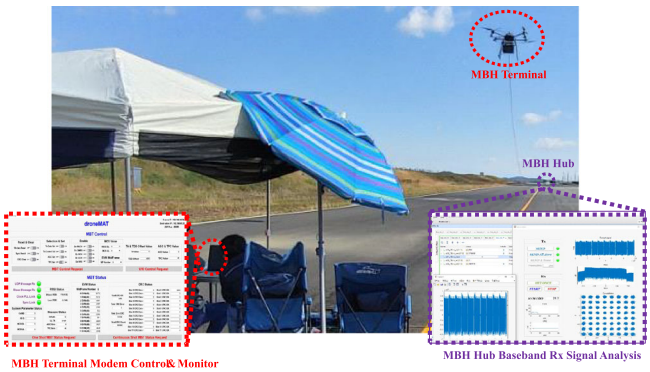

FIGURE 14 Mobile backhaul (MBH) link test environment with the modem analysis tool (MAT) and modem control tool (MCT) for monitoring and controlling.

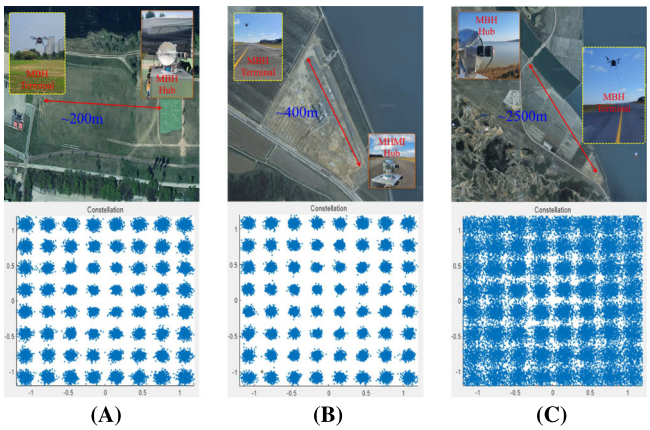

FIGURE 15 Mobile backhaul (MBH) link tests and the received constellations at various distances: (A) 200 m, (B) 400 m, and (C) 2.5 km.

22337326, 2023, 5, Downloaded from https://onlinelibrary.wiley.com/doi/10.4218/etrij.2023-0112 by Elect & Telecom Research, Wiley Online Library on [01/11/2023]. See the Terms and Conditions (https://onlinelibrary.wiley.com/terms-and-conditions) on Wiley Online Library for rules of use; OA articles are governed by the applicable Creative Commons License

In the second test environment shown in Figure 15B, without any scatterers present, all aspects, including the initial beam alignment, beam tracking, signal strength, and channel conditions, matched the predicted results. We achieved a peak data rate of 1.3 Gbps for MCS5 without errors and an EVM of approximately 26 dB.

Finally, in the third test environment shown in Figure 15C, with scatterers and reflection waves on a bridge railing near the MBH hub antenna, we received the anticipated signal strength, although the channel state was somewhat degraded. The initial beam alignment and tracking functions were effective; however, antenna movement was limited owing to the broad coverage width caused by the distance. The PER at MCS5 of the UL and DL fell below 0.1% and 0.2%, respectively, and achieved a peak data rate of 1.3 Gbps and an EVM of approximately 20 dB. Figure 15 also presents examples of the received constellations for all tested cases.

5.2 | UAV-BS integration test

Following the successful MBH link test, we performed an end-to-end (E2E) 5G communication test to demonstrate the viability of using MBH as a wireless backhaul for 5G-NR FBS (gNB) deployed in air. This test utilized a commercial 5G-NR UEs, a 5G-NR FBS, 5G core network (5GCN) emulator, application server, and set of MBH hubs and terminals.

Figure 16 illustrates the network configuration used for this test. The local site on the ground consisted of an application server, 5GCN, and MBH hub. At a remote site where the 5G-NR UEs are located on the ground, the UAV was equipped with an integrated 5G-NR FBS and MBH terminal that hover over the UEs. To facilitate the E2E communication test, the application server was responsible for transmitting and receiving data traffic and streaming full-definition (FHD) videos. The 5GCN, which

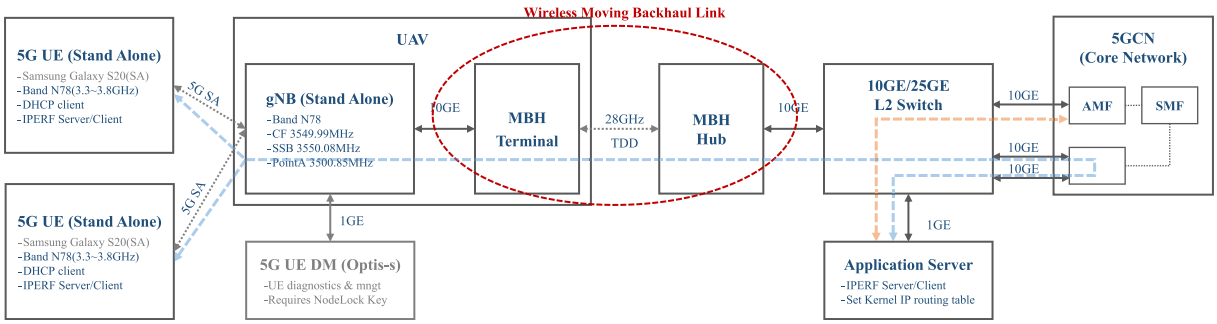

FIGURE 16 Configuration for uncrewed aerial vehicle base station (UAV-BS) integration test.

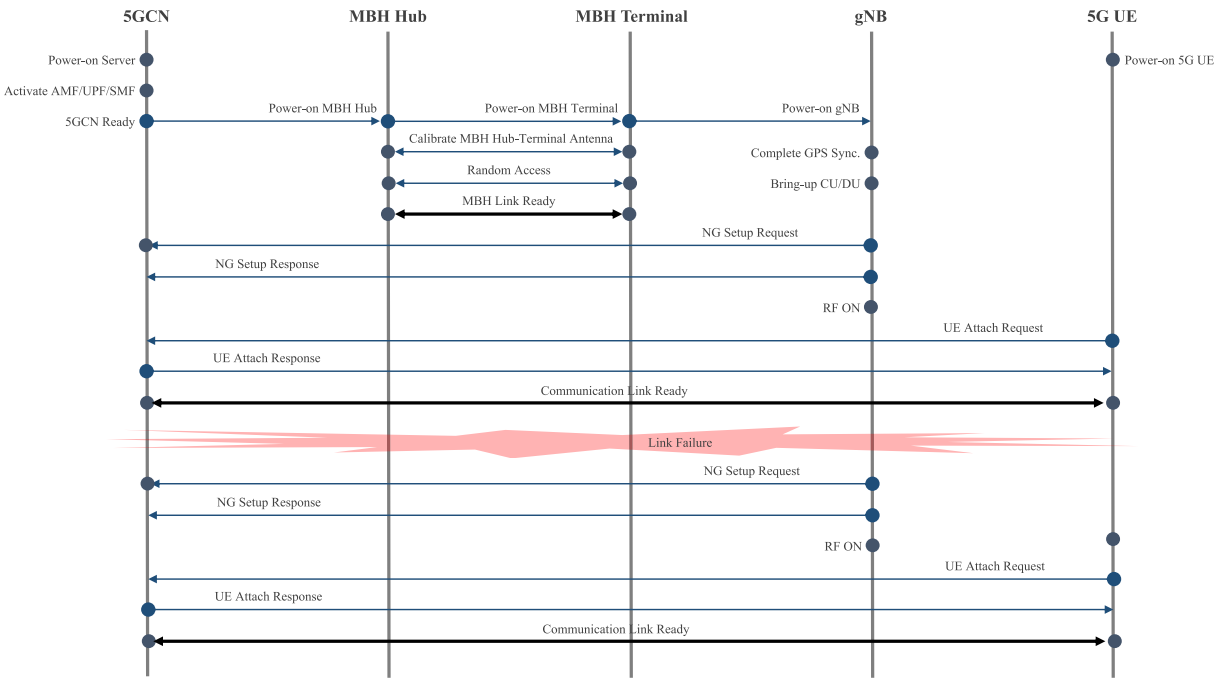

FIGURE 17 Uncrewed aerial vehicle base station (UAV-BS) integration test procedure.

22337326, 2023, 5, Downloaded from https://onlinelibrary.wiley.com/doi/10.4218/etrij.2023-0112 by Elect & Telecom Research, Wiley Online Library on [01/11/2023]. See the Terms and Conditions (https://onlinelibrary.wiley.com/terms-and-conditions) on Wiley Online Library for rules of use; OA articles are governed by the applicable Creative Commons License

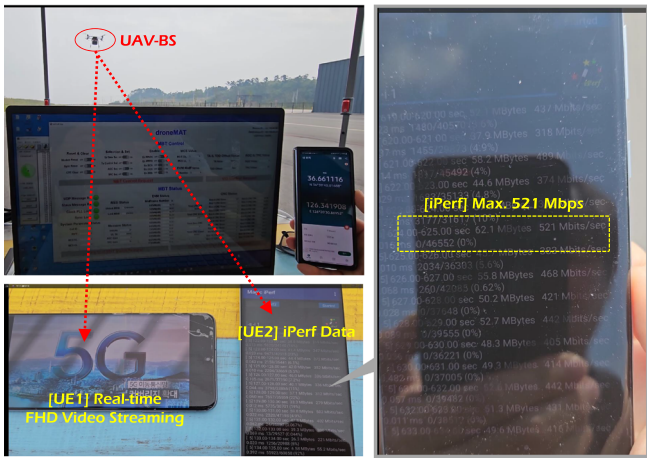

FIGURE 18 Uncrewed aerial vehicle base station (UAV-BS) integration test for mobile backhaul (MBH) wireless link of 5 km.

operates on a commercial Linux server, performed software-based user plane function (UPF), access and mobility management function (AMF), and session management functions (SMF). The 5GCN was connected to both the application server and MBH hub through a 10G Ethernet switch utilizing SFP+ connectors for the connection. As outlined in Section 3, the MBH hub and terminal establish a wireless backhaul link utilizing a signal bandwidth of 400 MHz in the mmWave band (26.5 GHz–27.3 GHz). The connection between the MBH terminal and the 5G-NR FBS was established via a 10G Ethernet interface. By contrast, the radio access network (RAN) between the 5G-NR FBS and 5G-NR UEs operated in the n78 band, licensed to Korea Telecom (KT). The 5G-NR FBS supported UE connections of up to 32 simultaneously during this test, and two UEs were utilized. We used a commercial standalone 5G-NR smartphone (Samsung Galaxy S20) as the UE. To maintain a reliable link connection between the UEs and the 5GCN, even in challenging degraded MBH wireless backhaul link scenarios caused by obstacles or strong winds, the 5G-NR FBS periodically attempted NG setup to re-establish the connection with the 5GCN, as depicted in Figure 17. UAV-BS integration tests were conducted at several locations around Drone Park in Daejeon and UV Land in Taean, Korea, where the LoS channels between MBH hubs and terminals can be established, as depicted in Figure 15. The test results demonstrated an E2E data traffic throughput from the application server to a UE of 700 Mbps when the link distance between the MBH hub and terminal was less than 2.5 km. Note that the MBH wireless backhaul link can support a maximum of 1.3 Gbps, as mentioned in Section 5.1. However, during this test, the 5G-NR FBS, which is still in its development phase, led to a maximum traffic rate of 700 Mbps. An additional UAV-BS integration test was performed under a 5 km LoS channel between the MBH hub and the terminal. The test results revealed an average data traffic transmission rate of 500 Mbps, measured using the iPerf tool, from the application server to one of the two UE devices. Simultaneously, real-time FHD video streaming from the application server was successfully achieved, specifically targeting another UE, as illustrated in Figure 18.

6 | CONCLUSIONS

In this study, we presented the implementation of an mmWave backhaul for UAV-BSs that offers high capacities over long distances. Our MBH system demonstrated a maximum throughput of 1.3 Gbps over a distance of 2.5 km, and a data rate of 300 Mbps, even within a range of 10 km. The use of a narrow beam with beam alignment for long-distance communication was crucial to achieving our goals. We also provided details of our testbed setup, including the baseband modem, RF, and antenna components, and we presented field test results that confirm the functionality and performance of the system.

Our UAV-BS system addresses key challenges to providing temporary wireless network services in areas where traditional communication infrastructures are not available; hence, it has significant potential for use in disaster relief efforts, remote locations, and other scenarios where communication services are vital. Moreover, our system can play an important role in communication systems for 5G and beyond because UAV-BSs are expected to be key components of NTNs.

CONFLICT OF INTEREST STATEMENT

The authors declare that there are no conflicts of interest.

ORCID

Seungjae Bahng https://orcid.org/0009-0005-5907-4965

REFERENCES

1. G. Geraci, D. Lopez-Perez, M. Benzaghta, and S. Chatzinotas, *Integrating terrestrial and non-terrestrial networks: 3D opportunities and chanllenges*, arXiv preprint, 2022. https://doi.org/10.48550/arXiv.2207.10385
2. X. Lin, S. Rommer, S. Euler, A. Yavuz, and R. Karlsson, *5G from space: an overview of 3GPP non-terrestrial networks*, IEEE Commun. Stand. Mag. **5** (2021), no. 4, 147–153.
3. 3GPP: *Unmmaned aerial system (UAS) support in 3GPP*, TS 22.125, 2022.
4. S. Mohsan, M. Khan, F. Noor, I. Ullah, and M. Alsharif, *Towards the unmanned aerial vehicles (UAVs): a comprehensive review*, Drones **6** (2022), no. 6, 1–27.
5. Y. Zeng, R. Zhang, and T. J. Lim, *Wireless communications with unmanned aerial vehicles: opportunities and challenges*, IEEE Commun. Mag. **54** (2016), no. 5, 36–42.
6. A. Merwaday, A. Tuncer, A. Kumbhar, and I. Guvenc, *Improved throughput coverage in natural disasters: unmanned*

22337326, 2023, 5, Downloaded from https://onlinelibrary.wiley.com/doi/10.4218/etrij.2023-0112 by Elect & Telecom Research, Wiley Online Library on [01/11/2023]. See the Terms and Conditions (https://onlinelibrary.wiley.com/terms-and-conditions) on Wiley Online Library for rules of use; OA articles are governed by the applicable Creative Commons License

aerial base stations for public-safety communications, IEEE Veh. Technol. Mag. **11** (2016), no. 4, 53–60.
7. N. Zhao, W. Lu, M. Sheng, Y. Chen, J. Tang, F. Yu, and K. Wong, *UAV-assisted emergency networks in disasters*, IEEE Wireless Commun. **26** (2019), 45–51.
8. G. Castellanos, M. Deruyck, L. Martens, and W. Joseph, *Performance evaluation of direct-link backhaul for UAV-aided emergency networks*, Sensors **19** (2019), no. 15, 45–51.
9. B. Galkin, J. Kibilda, and L. A. DaSilva, *Backhaul for low-altitude UAVs in urban environments*, (IEEE International Conference on Communications (ICC), Kansas CIty, MO, USA), 2018, pp. 1–6.
10. 3GPP: *NR; integrated access and backhaul (IAB) radio transmission and reception*. TS 38.174, 2020.
11. A. Fouda, A. Ibrahim, I. Guvenc, and M. Ghosh, *UAV-based in-band integrated access and backhaul for 5G communications*, (IEEE 88th Vehicular Technology conference (VTC-FALL), Chicago, IL, USA), 2018, pp. 1–5.
12. H. Zhang, Z. Qi, J. Li, A. Aronsson, J. Bosch, and H. Olsson, *5G network on wings: a deep reinforcement learning approach to the UAV-based integrated access and backhaul*, arXiv preprint, 2023. https://doi.org/10.48550/arXiv.2202.02006
13. N. Ansari, D. Wu, and X. Sun, *FSO as backhaul and energizer for drone-assisted mobile access networks*, ICT Express **6** (2020), 139–144.
14. S. Nath, S. P. Singh, and S. Sengar, *Interference and noise analysis for hybrid FSO/RF-based 6G mobile backhaul*, ETRI J. **44** (2022), no. 6, 966–976.
15. 3GPP: *Unmanned aerial system (UAS) support in 3GPP*, TS 22.125. 3GPP, 2018.
16. MIST, *Evaluation results of communication service coverage and quality*, Republic of Korea, 2021.
17. 3GPP: *Base station (BS) radio transmission and reception*, TS 38.104, 2018.
18. 3GPP: *Evolved universal terrestrial radio access (E-UTRA); physical channels and modulation*, TS 36.211, 2021.
19. Y. Jeon, H. Park, and E. Choi, *Synchronization and cell search procedure in 3GPP 5G NR systems*, (21st International Conference on Advanced Communication Technology (ICACT), PyeongChang, Republic of Korea), 2019, pp. 475–478.
20. T. A. Pham and B. T. Le, *A proposed preamble detection algorithm for 5G-PRACH*, (International Conference on Advanced Technologies for Communications (ATC), Hanoi, Vietnam), 2019, pp. 210–214.
21. A. Finnerty and M. Lee, *Integrated SD-FEC in Zynq UltraScale + RFSoCs for higher throughput and power efficiency*, Xilinx white paper (WP498), 2018.

AUTHOR BIOGRAPHIES

Jangwon Moon received his BS degree in Electronics Engineering from the Shibaura Institute of Technology, Tokyo, Japan, in 2007 and his MS degree in Wireless Communication from Waseda University in Tokyo, Japan in 2009. Since 2010, he has worked with the Electronics and Telecommunications Research Institute in Daejeon, Republic of Korea, as a senior engineer. His primary research interests include wireless communication systems, VLSI, on-chip communication architectures, and various modern designs.

Junwoo Kim received his BS degree in Electronics Engineering from Kyungpook National University, Daegu, Republic of Korea, in 1996, his MS degree from the Korea Advanced Institute of Science and Technology in Daejeon, Republic of Korea in 1998 and his PhD degree from Chungnam National University in Daejeon, Republic of Korea in 2013. He was a researcher at the Dacom Corporation from January 1998 to September 2001. Since October 2001, he has worked at the Electronics and Telecommunications Research Institute in Daejeon, Republic of Korea, where he is currently a principal engineer with a wireless transmission research team. His main research interests include VSLI, on-chip communication architectures, and various modern designs.

Hoon Lee received his MS degree in Electrical Engineering from the School of Electrical Engineering, Jeonbuk National University, Jeonju, Republic of Korea, in 1997. Since 1999, he has worked with the Electronics and Telecommunications Research Institute in Daejeon, Republic of Korea, where he is currently a principal researcher. His main research interests include wireless transport networks, 5G/6G mobile communication systems, network architectures, and technologies to expand mobile communication service coverage in mmWave/Sub-THz.

YoungJin Moon received his BS degree in Electronics Engineering from Kyungpook National University, Daegu, Republic of Korea, in 1996, and his MS degree in Information Communication Engineering from GIST in Gwangju, Republic of Korea in 1999. Since July 1999, he has worked at the Electronics and Telecommunications Research Institute in Daejeon, Republic of Korea, where he works as a principal engineer with a wireless transmission research team. His main research interests include VSLI, on-chip communication architectures, and various modern designs.

22337326, 2023, 5, Downloaded from https://onlinelibrary.wiley.com/doi/10.4218/etrij.2023-0112 by Elect & Telecom Research, Wiley Online Library on [01/11/2023]. See the Terms and Conditions (https://onlinelibrary.wiley.com/terms-and-conditions) on Wiley Online Library for rules of use; OA articles are governed by the applicable Creative Commons License

Yongsu Lee received his BS and MS degrees in Electronics from Kyungpook National University, Daegu, Republic of Korea, in 1996 and 1998, respectively, and his PhD degree in Electronics from Chungnam National University in Daejeon, Republic of Korea, in 2011. Since 2000, he has been with the Terrestrial and Non-Terrestrial Integrated Telecommunications Research Laboratory at the Electronics and Telecommunications Research Institute (ETRI), Daejeon, Republic of Korea. His research areas include mobile communication. Prior to joining ETRI in 2000, he worked for the Agency for Defense Development (ADD) in Daejeon, Republic of Korea, where he was involved in the development of an antiship cruise missile system.

Youngjo Bang received his MS and PhD degrees in Electrical Engineering from the Korea Advanced Institute of Science and Technology, Daejeon, Republic of Korea, in 1991 and 1997, respectively. In 1997, he joined the Electronics and Telecommunications Research Institute in Daejeon, Republic of Korea, where he is currently a principal member of the research staff. His research interests include 5G/6G mobile communications, mmWave beamforming, and moving backhaul systems.

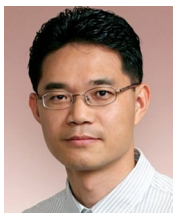

Kyungyeol Sohn received his BS and MS degrees in Electronic Engineering from Kon Kuk University, Seoul, Republic of Korea, in 1992 and 1994, respectively. Since 1994, he has worked with the Electronics and Telecommunications Research Institute, Daejeon, Republic of Korea, as a principal researcher. His research interests include wireless communication systems and embedded HW/SW designs.

Jungsook Bae received her BS, MS, and PhD degrees in Computer Engineering from Chungnam National University, Daejeon, Republic of Korea, in 1994, 1996, and 2007, respectively. Since 1999, she has worked on mobile communication systems at the Electronics and Telecommunications Research Institute in Daejeon, Republic of Korea. As part of the chief technical staff, she now leads a development of movable high-capacity mobile communication infrastructure for telecommunication disaster and rescue research project. Her main research interests include 5G/6G mobile communications, V2X, and communication technologies for UAM.

Kwangseon Kim received his BS and MS degrees in Electronic Engineering from the School of Electrical Engineering, Kyungpook National University, Daegu, Republic of Korea, in 1998 and 2000, respectively. Since 2000, he has worked at the Electronics and Telecommunications Research Institute in Deajeon, Republic of Korea, where he is currently a principal researcher. His main research interests include millimeter wave/THz RF transceiver design and the system-level integration of transceivers and RF components.

Seungjae Bahng received his BS, MS, and PhD degrees from Inha University, Incheon, Republic of Korea, Gwangju Institute of Science and Technology, Republic of Korea, and the University of Hawaii, USA in 1998, 2000, and 2005, respectively. He joined the Electronics and Telecommunications Research Institute in Daejeon, Republic of Korea, in 2005, where he currently works as a principal researcher in the Intelligent Wireless Access Research Section. His research interests include wireless communication systems and real-world applications.

Heesoo Lee received his BS, MS, and PhD degrees in Industrial Engineering from the Korea Advanced Institute of Science and Technology, Daejeon, Republic of Korea, in 1993, 1995, and 2001, respectively. In 2001, he joined the Electronics and Telecommunications Research Institute in Daejeon, Republic of Korea, where he is currently the Director of the Intelligent Wireless Access Research Section. He works on core technologies for future wireless cellular communications, especially in the areas of artificial intelligence, millimeter waves, OFDM, SC-FDMA, multiuser MIMO, interference management, and relay.

How to cite this article: J. Moon, J. Kim, H. Lee, Y. Moon, Y. Lee, Y. Bang, K. Sohn, J. Bae, K. Kim, S. Bahng, and H. Lee, *Implementation of mmWave long-range backhaul for UAV-BS*, ETRI Journal **45** (2023), 781–794. DOI 10.4218/etrij.2023-0112

22337326, 2023, 5, Downloaded from https://onlinelibrary.wiley.com/doi/10.4218/etrij.2023-0112 by Elect & Telecom Research, Wiley Online Library on [01/11/2023]. See the Terms and Conditions (https://onlinelibrary.wiley.com/terms-and-conditions) on Wiley Online Library for rules of use; OA articles are governed by the applicable Creative Commons License